Mesh Human Phantoms with MCNP

Casey A. Anderson, Karen C. Kelley, John T. Goorley

Los Alamos National Laboratory, Los Alamos, New Mexico, USA, 87545

Improvements in technology and computing have provided highly detailed representations of the human body for biomedical simulations. One specific application is the use of these computational phantoms for particle transport in MCNP, a general purpose particle transport code developed by Los Alamos National Laboratory (LANL). Traditional mathematical based phantoms, such as the ICRP 23 Reference Man, MIRD-5 Adult Male and the Snyder phantom, use equations to specify the surfaces and volumes of organs within the body. Image based models, such as the Visible Photographic Man (VIP-Man), Zubal model, and Extended cardiac-torso (XCAT), use segmented CT and MRI data to construct a three dimensional model of the body. Image based models required voxelization to run in MCNP, producing a tradeoff between anatomical accuracy and computational expense based on voxel size, while mathematical based models only provided a crude representation of the human anatomy. The most recent release of MCNP allows an unstructured mesh generated from Abaqus/CAE to be imported as an alternative geometry to the traditional constructive solid geometry (CSG). This capability can provide improved geometry and computational run time compared to mathematical and voxelized models. It also provides improved visualization capabilities, isolation by parts (for visualization and source specification), flux and dose information for each element, multiphysics finite element analysis (FEA) of the mesh, and the potential for patient specific models. This report demonstrates these new capabilities of MCNP, specifically the use of unstructured mesh human phantoms for health physics and medical applications.

1. Introduction

Computational human phantoms used for dose calculations require an appropriate geometry and realistic radiation interaction data conforming to the ICRP 23 Reference Man (Allisy 1992b; Snyder 1974). Traditional *Mathematical Models* use mathematical descriptions of planes and surfaces to create a representation of the human anatomy. Adjustments in these equations accommodate for population differences based on age, size, sex, and race. In the mid 1980s, *Tomographic Models* were developed using segmented image data from CT and MRI scans to reconstruct a three dimensional model of the body (Allisy 1992b). The complex surfaces from these models are often described using a series of data points and splines (Segars 2010).

Modeling the human anatomy with the ability to import into computer codes often requires a tradeoff between anatomical accuracy and computational expense. Mathematical models, such as the MIRD-5 Adult Male and Snyder phantom, are easily produced in MCNP legacy code, yet only provide a crude representation of the human anatomy (Allisy 1992b; Snyder 1969). The complex volumes and surfaces used in tomographic models can't easily be reproduced in MCNP legacy code, requiring the models to be voxelized and filled in an MCNP lattice (Lee 2008). The voxelization process produce large, expensive models or small, less detailed models based on the voxel seed size (Xu 2000).

The general purpose Monte Carlo transport code MCNP, developed at Los Alamos National Laboratory, has a new capability that allows particle transport with hybrid geometries (Goorley 2011). Unstructured mesh generated from Abaqus/CAE can be included in the same model with the legacy CSG geometry. Models developed with Computer Aided Engineering (CAE) software no longer need to be voxelized or rewritten in MCNP legacy input, saving many man-hours of conversion time while maintaining the native geometry. This paper discusses the use of hybrid geometries with unstructured mesh human phantoms in MCNP, specifically for comparison, validation and verification (V&V) and dose calculations.

2. Methods and Materials

The newest release of the general purpose Monte Carlo radiation transport code MCNP, version 6 (MCNP6), is used to demonstrate the new unstructured mesh capability for phantoms in hybrid geometries. Several voxelized computational phantoms were used for testing: the Snyder Head phantom (Snyder 1969), the Zubal Head (Zubal 1994), and the VIP-Man (Xu 2000). These models have been previously tested in MCNP (Goorley 2002; Xu 1998) and are common phantoms for medical physics applications (Goorley, 2005). Meshes were generated by reconstructing voxelized models of the phantoms into a hexahedra mesh and by the standard meshing tools in Abaqus/CAE. Both mesh types were used in the hybrid geometry testing. The following sections describe the MCNP hybrid geometry capability, several phantoms used in testing, and the python script that converts voxelized phantoms into mesh inputs.

2.1 MCNP6 Hybrid Geometry

The Monte Carlo development team at Los Alamos National Laboratory has been developing the particle transport code MCNP for over 40 years, with the most recent release being MCNP6. Abaqus/CAE is a Computer Aided Engineering (CAE) software developed by Simulia and Dassault Systèmes, used for designing models for finite element analysis (Simulia). MCNP6 reads in the mesh data from the Abaqus/CAE generated input file and creates a global mesh model that is embedded in a mesh universe. A mesh universe in CSG is required for particle transport; other CSG geometries may also be included. Particle tracking occurs through the mesh and CSG universe, and spatial, energy, and time dependent flux and energy deposition values are written to an elemental edits (.eeout) file (Goorley 2011). The elemental edits file can then be converted into an ODB file, viewed in Abaqus/CAE, and provide a source term for further multiphysics analysis.

2.2 Computational Phantoms

The development of computational phantoms for radiation dosimetry has been around since the 1960s (Allisy 1992b), increasing in complexity and detail as computer resources evolve. Full body models have been developed to accommodate for the size differences encountered in the general population; factors include weight, BMI, race, sex, age, and pregnancy (Xu, 2010; Snyder 1974). Mathematical phantoms account for these differences by adjusting the equations and surfaces as needed (Lee 2008), while adjustments to tomographic models, though much more rigid, can also account for these differences (Xu, 2010). Dr. X. George Xu and several colleagues at RPI have made significant advances on computational phantoms for medical purposes, many published in

the handbook *Handbook of Anatomical Models for Radiation Dosimetry* (Xu 2009; Xu, 2010). Calculations of dose and interactions in the body requires accurate tissue data, found in the *ICRP Report 23 Reference Man*, and radiation interaction data, found in the *ICRU Report 46* (Allisy 1992a; Snyder 1974). Several of the computational phantoms used in this paper are described below. The Mathematical Internal Radiation Dosimetry (MIRD) mathematical computational phantom, commonly used for dose assessment, is shown to the far left in Figure 1(a).

2.2.i The Visible Photographic Man

The National Library of Medicine (NLM) has been developing anatomically detailed, three-dimensional representations of the male and female adult human bodies in the Visible Human Project (VHP) (NLM, 2011). The VIP-Man is *an image based whole-body adult male model constructed from color photographs of the Visible Human Project* (Xu 2000). Voxelized modes of the VIP-Man, ranging in size from 0.33 mm x 0.33 mm x 1 mm resolution (3.7 billion voxels) to 4 mm x 4 mm x 4 mm resolution (5.9 million voxels) were developed for use in MCNP. The 4 mm model is commonly used as an optimized model for computational efficiency and accuracy (Xu, 1998). Mesh models of the 4 mm resolution VIP-Man are shown in Figure 1 (b & c).

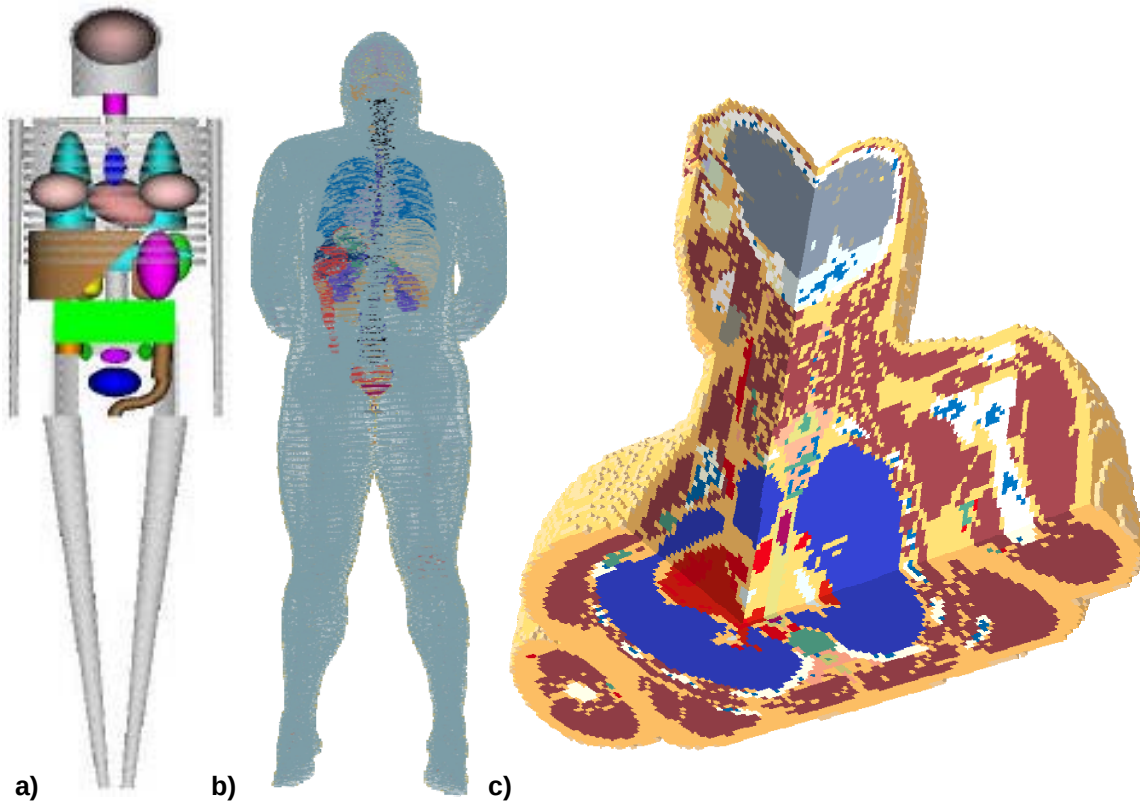

Figure 1: The mathematical MIRD-5 Adult Male (a) and the tomographic 4 mm VIP-Man (b,c)

2.2.ii Snyder & Zubal Head Phantom

The Snyder Head phantom is a mathematical model developed in the 1960s that uses three ellipsoid equations to represent the human head (Goorley 2008; Allisy 1992b; Snyder 1969). The equations below describe the Snyder Head phantom: equation 1 describes the brain boundary; equation 2 describes the skull boundary; equation 3 defines the scalp boundary. Voxel models of this phantom were developed and used in MCNP for reference dosimetry calculations (Goorley 2002). An analytical solid model was generated in Abaqus/CAE using equations 1-3 and meshed with various element types and seed sizes. The Snyder Head was compared with analytical CSG, voxelized CSG, voxelized mesh, and unstructured mesh models. The Zubal Head phantom, named after one of the original developers Dr. George Zubal, is a tomographic model developed in the 1990s at Yale University (Zubal 1994). The voxelized head section of the Zubal Head is shown to the left in Figure 2.

$$\left(\frac{x}{6}\right)^2 + \left(\frac{y}{9}\right)^2 + \left(\frac{z-1}{6.5}\right)^2 = 1 \qquad (1)$$

$$\left(\frac{x}{6.8}\right)^2 + \left(\frac{y}{9.8}\right)^2 + \left(\frac{z}{8.3}\right)^2 = 1 \qquad (2)$$

$$\left(\frac{x}{7.3}\right)^2 + \left(\frac{y}{10.3}\right)^2 + \left(\frac{z}{8.8}\right)^2 = 1 \qquad (3)$$

2.2.iii. Other Phantoms

There are many computational phantoms used today, many described in the ICRU Report 48, with newer versions described in the book *Handbook of Anatomical Models for Radiation Dosimetry, 1st edition* (Xu 2009; Allisy 1992b). Some of these models include; the RPI-Adult Male (RPI-AM), RPI-Adult Female (RPI-AF), RPI-Pregnant Female (RPI-P), Female Adult mesh (FASH), Male Adult mesh (MASH), Virtual Family (Szczerba 2010), NORMAN phantom, the Korean, Japanese, and Chinese Computational Phantoms, and the MIRD phantoms (Allisy 1992b). The NURBS-based, Extended, and Mathematical cardiac-torso (NCAT, XCAT, MCAT, respectively) phantoms are based on the Visible Human Project from the NLM, similar to the VIP-Man, and provide imaging simulation (XCAT, MCAT) and 4D respiratory modeling (NCAT) (Segars 2010). This large selection of computational human phantoms will ideally be tested with the hybrid geometry capability of MCNP.

2.3 Voxel to Abaqus Script

Without solid models of these image based phantoms readily available, an alternate mesh generating process was used. A python script was developed that extracts data from the MCNP lattice geometry, generates an Abaqus/CAE mesh input file, and uses built in methods in Abaqus/CAE to merge the nodes, renumber the elements, and write a mesh input file. Each integer represents an element within in a part, and the default parts names correspond to the integer they represent (1=ONE, 2=TWO, etc.). A separate file can be included in the command line arguments that references an integer to a name, naming the parts as indicated (1=BONE, 2=FAT, etc.). The MCNP lattice model and reconstructed Abaqus/CAE unstructured mesh model are the exact same geometry, and provide good benchmarks for testing and comparison. These files are readable by

Abaqus/CAE, separated into parts, and capable of running in MCNP6 with adjustments to the MCNP input deck. Comparison of the lattice geometry viewed with the native MCNP plotter and the mesh viewed in Abaqus/CAE are shown on the right in Figure 2.

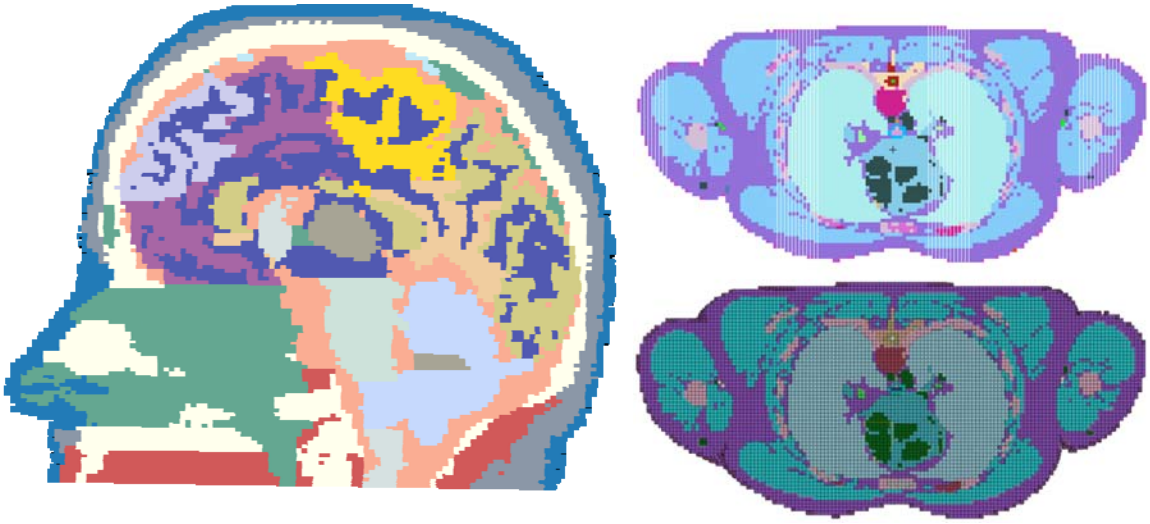

Figure 2: Zubal Head Phantom viewed in Abaqus/CAE (left); Transverse slice of the 4 mm VIP-Man viewed in MCNP (top right) and in Abaqus/CAE (bottom right)

3. Results

In this paper, we present the initial findings of using human phantom hybrid geometries for particle transport in MCNP6. Computational results were performed on Linux OS (RedHat) and a 2.67 GHz Intel Xeon processor Model X7542 using runs with eight processors. Converting the MCNP voxel data into an Abaqus/CAE mesh with the python script took several minutes for the 8 mm Snyder Head model and up to 11 hours for the 4 mm VIP-Man, using approximately 200 MB of memory for each process. The largest MCNP lattice tested was 155 million elements, taking 3 days and 11 GB memory to generate the mesh. The meshed model file sizes were larger than the CSG counterparts: the Zubal Head model 200 times larger, both VIP-Man models 40 times larger, and the Snyder models (both 4 mm and 8 mm) only three times larger. MCNP requires a completely filled lattice, so many voxels outside the geometry of interest can be removed from the mesh model, specifically the surrounding air voxels. This reduces file sizes by nearly 50% and significantly improves the computational efficiency. File sizes and mesh data of the voxelized CSG and mesh models are compared in Table 1.

The voxelized hybrid geometries require longer run times for processing the geometry and particle tracking than their voxelized CSG counterparts, shown in Table 2. However, the unstructured mesh generated from Abaqus/CAE improved computer run time compared to the voxelized mesh models, specifically shown in the solid Snyder Head phantom. MPI pre-processing allowed parallel processing on separate parts, partially explaining the faster setup time of the larger 41-part VIP-Man compared to the slow setup of the 5-part male pelvis model. The voxelized CSG Snyder

Head phantoms were not represented by a repeated lattice and had a large number of parts for relatively few elements, resulting in a comparatively faster pre-processing time with the hybrid geometry. Only the Snyder Head phantom was completely tested with and without the surrounding air voxels, while others were tested for pre-processing. Removal of these elements sped up pre-processing on the larger models, such as the Zubal head and VIP-Man, with only slight improvements on the smaller Snyder models. Current limitations with the hybrid geometries include a lack of variance reduction, used to increase computational efficiency, and no neutron KERMA factors, used to convert energy deposition to absorbed dose. All variance reduction and KERMA factors were removed from the CSG models for accurate comparisons.

Table 1: Abaqus Mesh Data from CSG voxelized models and File Size Comparisons

Model	**Mesh Data***			**Geometry File Size (MB)**		
	Parts	**Voxels**	**Volume**	**CSG**	**Mesh**	**Mesh***
VIP-Man (Head/Torso)	41	321958	10421	4.3	178.6	53.0
VIP-Man (Whole Body)	61	1628350	20605	19.3	830.2	270.1
Zubal Head	61	543338	3381.7	0.7	150.9	82.6
Snyder Head (8mm)	64	6488	3321.9	0.9	2.98	1.8
Snyder Head (4mm)	40	47448	3036.7	5.2	16.5	10.7
Snyder Head (UM)	3	13018	2751.4	---	---	1.6

* Mesh Data with the air voxels removed from the geometry

Table 2: Run Times for Processing and Transport (100 million histories)

Model	**Processing (min)**			**Transport (min)**		
	CSG	**Mesh**	**Mesh***	**CSG**	**Mesh**	**Mesh***
VIP-Man (Head/Torso)	1.0	998.2	25.2	1551	---	19006
VIP-Man (Whole Body)	4.8	----	605.5	1187	----	36171
Zubal Head	0.9	411.1	18.7	2688	----	19715
Snyder Head (8mm)	0.2	0.3	0.2	1204	78509	17804
Snyder Head (4mm)	0.5	0.6	0.5	5490	----	64580
Snyder Head (Analytic)	0.1	----	0.1	11930	----	14847
Lungs (4mm)	---	----	2.7	---	----	1173
Lungs (UM)	---	----	0.3	---	----	539

* Mesh Data with the air voxels removed from the geometry

Table 3: Optimization of the 4mm VIP-Man

Mesh Data of the sectioned VIP-Man			Computer Run Time*		
Parts	**MAX Elements per Part**	**AVG Elements per Part**	**Pre-processing (min)**	**Transport (min)**	**Memory (GB)**
61	645491	26700	605.6	36171	2.0
99	72543	16450	34.9	19807	3.1
139	72543	11712	28.1	19411	3.5
142	54709	11476	26.4	**TBD**	4.4

*** Computer Run Times per CPU for 100 million histories: TBD - To Be Determined**

A significant limiting factor in processing the hybrid geometries is the number of elements for each part; where greater than 50,000 elements in a part produces a large increase in computer expense. The full model of the VIP-Man contained 650,000 elements for the fat and muscle sections, requiring over 10 hours for pre-processing. Adjustments in the python conversion script separated these large parts into multiple smaller parts, reducing the maximum number of elements per part to 73,000 and 55,000 elements. Increasing the number of parts increased the memory footprint while also showing significant improvements in pre-processing and transport time, shown in Table 3. The large memory required is limiting the ability to achieve transport results in the mesh, and is currently being evaluated for the 142 part VIP-Man.

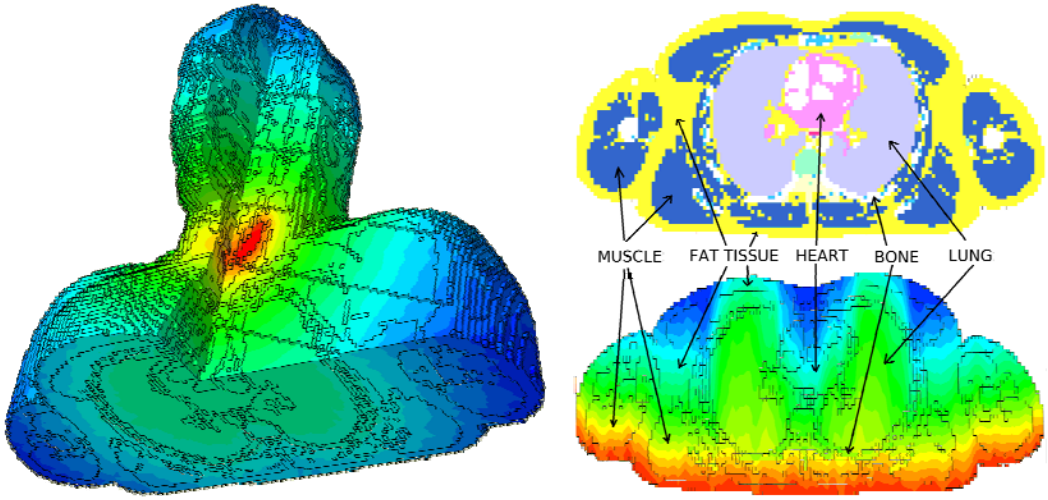

Figure 3: Simulating an Iodine source in the thyroid (left) and a posterior-anterior directional gamma source (right)

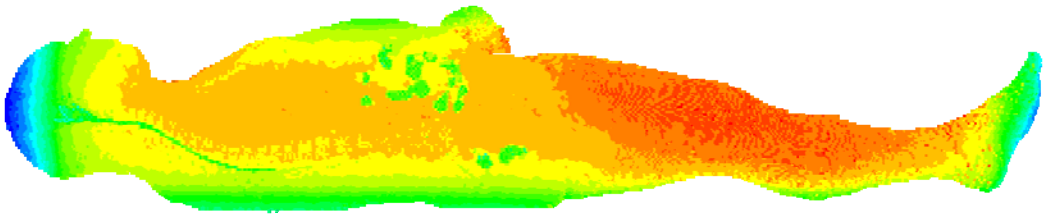

Figure 4: Whole body gamma irradiation source of the 4 mm VIP-Man

The Snyder Head models used a 10 cm diameter gamma beam as the source (Goorley 2008). The Zubal Head phantom used this same source and was compared with the Snyder model since they represent the same section of the human body. The head and torso models of the VIP-Man used a posterior-anterior directional photon source, shown to the right in Figure 3. The anatomy shows the particle interaction with specific body parts, specifically lower attenuation through air in the lungs and higher attenuation through the dense muscle. An Iodine source in the thyroid, a treatment used for hyperthyroidism, is used to demonstrate the volume source capability with MCNP6, and is shown to the left in Figure 3. As the largest model, the complete VIP-Man was irradiated using a whole body source to achieve converged results for each element within the model, shown in Figure 4.

The unstructured mesh models tested were the lungs of the VIP-Man and the Snyder Head phantom, both generated by meshing a solid model in Abaqus/CAE. The Snyder head phantom was meshed with hexahedra to 0.8% of the analytic volume (2771 cm^3), and compared with the voxelized mesh models with the same source. Both unstructured models showed computational improvements compared to the voxelized models; the unstructured mesh lungs took half the time as the voxelized lungs, and the unstructured Snyder Head was faster and more geometrically accurate than the 4 mm voxelized model. An analytical model of the Snyder Head phantom was tested in legacy CSG, and was slightly faster than the unstructured mesh model for transport. The results of the hybrid geometry runs on the Snyder Head are shown below in Figure 5, which include the 4 mm, 8 mm, and unstructured mesh models. The unstructured chest and lungs model, which had an isotropic gamma source placed between the lungs, is shown in Figure 6.

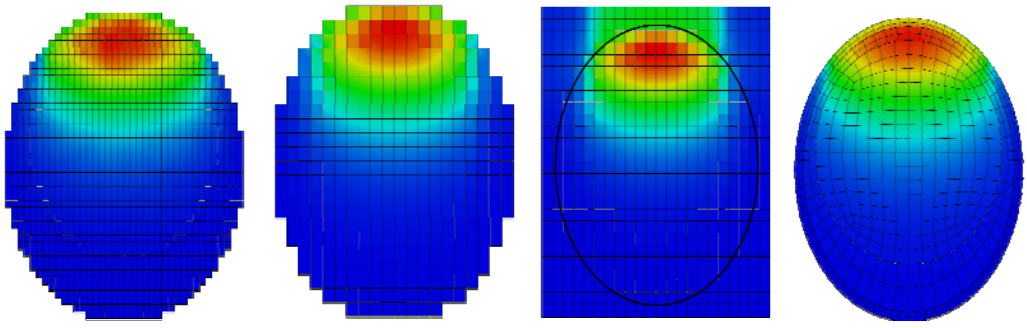

Figure 5: 10 cm diameter mono-directional beam on the Snyder head phantoms. From left to right: 4 mm voxelized model, 8 mm voxelized model, 8 mm voxelized model including surrounding air voxels, unstructured mesh model generated from Abaqus/CAE.

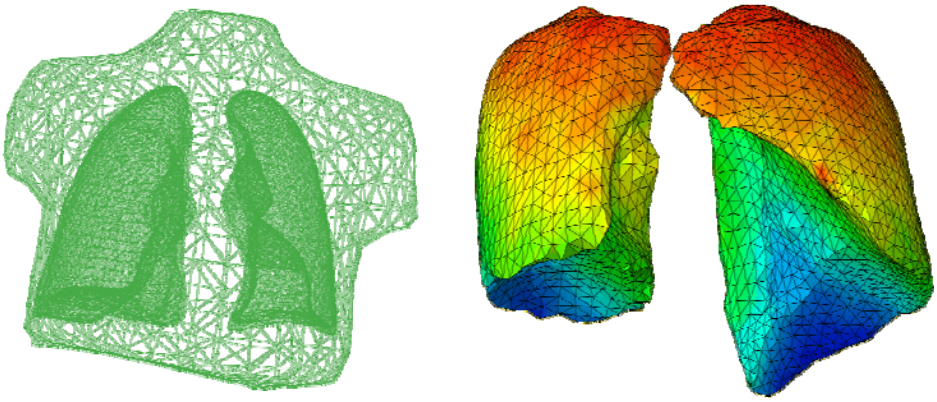

Figure 6: Unstructured mesh representation of the chest & lungs of the VIP-Man (left) and a gamma irradiation source of the lungs (right)

Mesh tallies offer the ability to tally particle flux or energy deposition within the mesh, and provide a direct comparison between CSG and hybrid geometries. Comparisons of the mesh tallies of the voxelized mesh and voxelized CSG 8 mm Snyder model are shown below in Figure 7, showing the relative statistical error for 1 million and 100 million histories between the two results. The x-axis represents the instance in the mesh tally, and the y axis the difference between the two tallies. While the results show a nearly 10% statistical difference for 1 million histories, they converge to 0.35% for 100 million histories. A similar convergence was obtained between the Snyder Head mesh model with and without the surrounding air voxels, with 0.31% difference between both runs for 100 million histories. The behavior of the Monte Carlo method is also shown in Figure 8; as more particles enter an element, a larger sampling is received resulting in a lower statistical error. Areas nearest to the incident radiation receive more particles and a higher dose. The specific behavior of the dose-error plot is $N^{-1/2}$, where N is the number of sample particles, shown for 1 million and 100 million histories. The dose is normalized to each incident particle, explaining the same dose range for 1 million and 100 million histories.

4. Discussion

This paper discusses the implementation of unstructured mesh human phantom geometries as use for particle transport. Mesh tallies showed statistical agreement between voxelized CSG, voxelized mesh, analytical CSG, and unstructured mesh models of the Snyder Head phantom. Large models fared the worst computationally when comparing the hybrid and CSG voxelized geometries, partially due to the large number of elements for each part. Reducing the number of elements per part provided significant improvement in the pre-processing and transport of the models. Areas outside the geometry of interest that do not contribute to the overall dose, such as the legs and air voxels, can be removed from the geometry to increase the computer time. Voxelized hybrid models took longer computationally than their CSG counterparts, though the Abaqus/CAE generated meshes compared closely to analytical and voxelized CSG models. Outdated and voxelized models were used for testing this hybrid geometry capability, and are not demonstrating any significant breakthroughs in the use of computational phantoms for particle transport. The use of a complete unstructured mesh human phantom is needed to complete this study.

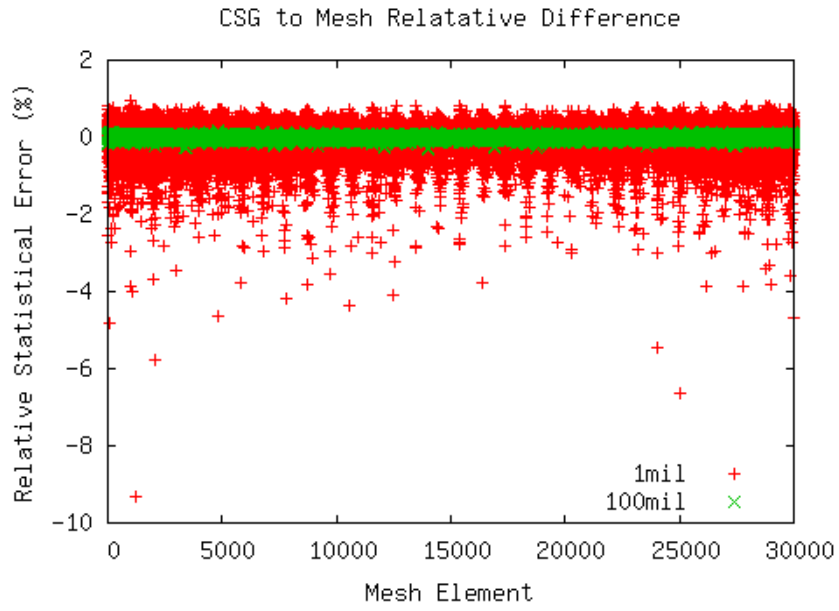

Figure 7: Mesh Tally Relative Statistical Error between the Abaqus and CSG voxelized models for 1 million (red) and 100 million histories (green). The X axis denotes the number of the mesh element

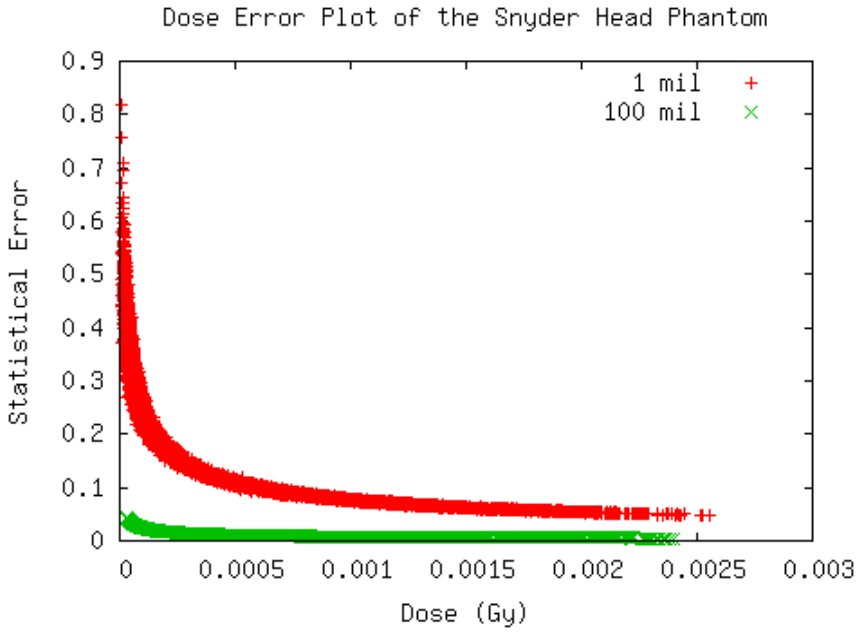

Figure 8: Dose Error plot of the 10 cm diameter irradiation source on the voxelized Snyder Head mesh model for 1 million (red) and 100 million (green) histories

5. Future Work

The improved versions of the VIP-Man are being tested and compared with the CSG voxelized models, including differences between running MPI and threaded versions of MCNP. Dose calculations from an Iodine-131 thyroid treatment are being calculated and compared with standard values; specific calculations include the dose to the prostate and other organs of interest from different uptakes to the thyroid and liver. Solid models of the VIP-Man and XCAT phantoms are currently being evaluated for use with MCNP. The XCAT phantom was not originally designed for FEA, and like many other models developed with Computer Aided Design (CAD) software, has problems meshing and currently cannot be used in MCNP. Ideally a solid phantom model, such as the XCAT or VIP-Man, will be used for testing of this hybrid capability. Other voxelized phantoms are being converted and tested.

6. Conclusion

The use of unstructured meshed human phantoms has great potential for the advancement of computational medical physics applications. Computational human phantoms are used for a variety of medical applications, such as tissue/organ deformation following surgery (Mohamed, 2004), respiratory and biological modeling (Segars 2010), linear accelerator calibration and dose assessment (Allisy 1992b; Xu 2000; Snyder 1969; Zubal 1994), providing a gradually improving understanding of interactions within the human body. Patient specific meshed models could be used for Monte Carlo based treatment planning and post treatment analysis as a more accurate alternative to the mathematical based ray tracing technique currently used in many radiotherapy procedures (Xiong 2007). Detailed whole body phantoms and improved computational analysis can develop better tissue interaction data, specific absorbed fractions, and weighting factors for particles in the body. Combination analysis from surgical procedures, respiratory modeling, and radiotherapy treatment with the same patient data could be used in the near future. Further testing of this capability is needed, but currently shows promising results of using the next generation of computational human phantoms for dose calculations.

7. Acknowledgements

Dr. X. George Xu and Dr. Paul Segars have developed and provided models of the VIP-Man and XCAT phantoms, respectively. Roger Martz and David Crane have been on the code development side of the hybrid geometry capability, including the script to generate an ODB for visualization. Chelsea D'Angelo has been testing and developing samples of the hybrid geometry capability. A special thanks to everyone listed above and many others who helped contribute to this project.

8. References

1. A. Allisy, A. Kellerer, R. Caswell, G. Adams, K. Doi, L. Feinendegen, M. Inokuti, I. Isherwood, J. Mallard, H. Paretzke, H. Rossi, A. Wambersie, G. Whitmore, and L Taylor. *Photon, Electron, Proton and Neutron Interaction Data for Body Tissues; ICRU Report 46. ICRU Publications*, 1992a.

2. A. Allisy, A. Kellerer, R. Caswell, G. Adams, K. Doi, L. Feinendegen, M. Inokuti, I. Isherwood, J. Mallard, H. Paretzke, H. Rossi, A. Wambersie, G. Whitmore, and L Taylor. *Phantoms and Computational Models in Therapy, Diagnosis, and Protection; ICRU Report 48*. ICRU Publications, 1992b.

3. T. Goorley. MCNP Medical Physics Geometry Database, Los Alamos National Laboratory Reports, LA-UR-05-692, 2005.

4. T. Goorley, W. Kiger III, and R. Zamenhof. "Reference Dosimetry Calculations for Neutron Capture Therapy with Comparison of Analytical and Voxel Models" *Medical Physics*, 29:145–156, 2002.

5. T. Goorley, M. James, T. Booth, F. Brown, J. Bull, L.J. Cox, J. Durkee, J. Elson, M. Fensin, R.A. Forster, J. Hendricks, H.G. Hughes, R. Johns, B. Kiedrowski, R. Martz, S. Mashnik, G. McKinney, D. Pelowitz, R. Prael, J. Sweezy, L. Waters, T. Wilcox, and T. Zukaitis. *Initial MCNP6 Release Overview, Submitted to Nuclear Technology,* Los Alamos National Laboratory Report, LA-UR-11-05198. 2011.

6. C. Lee, D. Lodwick, J. Williams, and W. Bolch. "Hybrid Computational Phantoms of the 15-year Male and Female Adolescent: Applications to CT Organ Dosimetry for Patients of Variable Morphometry". *Medical Physics*, 35:2366–2382, 2008.

7. A. Mohamed and C. Davatzikos. "Finite Element Mesh Generation and Remeshing from Segmented Medical Images". ISBI'04, pages 420–423, 2004.

8. NLM. The Visible Human Project. http://www.nlm.nih.gov/research/visible/visible_human.html, Sept 2011.

9. W. Segars, G. Sturgeon, S. Mendonca, J. Grimes, and B. Tsui. "4D XCAT Phantom for Multimodality Imaging Research". *Medical Physics*, 37, 2010.

10. Simulia. Introduction to Abaqus Training Manual

11. W. Snyder, M. Ford, G. Warner, and Jr H. Fisher. "Estimates for Absorbed Fractions for Monoenergetic Photon Sources Uniformly Distributed in Various Organs of a Heterogeneous Phantom". *Journal of Nuclear Medicine*, 47, 1969.

12. W. Snyder, M Cook, E. Nasset, L. Karhausen, G. Howells, and I. Tipton. *Report of the Task Group on Reference Man: ICRP Publication 23*. Pergamon Press, 1974.

13. D. Szczerba, E. Neufeld, M. Zefferer, G. Szekely, and N. Kuster. "Unstructured mesh generation from the virtual family models for whole body biomedical simulations". *Procedia Computer Science*, 1:837–844, 2010.

14. W. Xiong, D. Huang, L. Lee, J. Feng, K. Morris, E. Calugaru, C. Burman, J. Li, and C. Ma. “Implementation of Monte Carlo Simulations for the Gamma Knife System”. *Journal of P*hysics: Conference Series, 74, 2007.

15. X. Xu. Recent Progress on Computational Phantoms and Applications to Imaging and Therapy, 2010.

16. X. Xu and Keith F. Eckerman. *Handbook of Anatomical Models for Radiation Dosimetry, 1st edition*. Taylor & Francis, 2009.

17. X. Xu and B. Wang. “Issues Related to the Use of MCNP Code for an Extremely Large Voxel Model VIP-MAN”. 98(E2):3247–3259.

18. X. Xu, T. Chao, and A. Bozkurt. VIP-Man: “An Image-based Whole-body Adult Male Model Constructed from Color Photographs of the Visible Human Project for Multi-Particle Monte Carlo Calculations”. *Health Physics*, 78:476–486, 2000.

19. I. Zubal, C. Harrell, E. Smith, Z. Rattner, G. Gindi, and P. Hoffer. “Computerized Three-Dimensional Segmented Human Anatomy”. *Medical Physics*, 21:299–302, 1994.